Journal of Molecular Structure 983 (2010) 82–92

Contents lists available at ScienceDirect

Journal of Molecular Structure

journal homepage: www.elsevier.com/locate/molstruc

Properties of new low melting point quaternary ammonium salts with bis(trifluoromethanesulfonyl)imide anion

Minna Kärnä, Manu Lahtinen *, Anna Kujala, Pirkko-Leena Hakkarainen, Jussi Valkonen

Department of Chemistry, University of Jyväskylä, P.O. Box 35, FI-40014 Jyväskylä, Finland

ARTICLE INFO

Article history:
Received 12 August 2010
Accepted 12 August 2010
Available online 22 August 2010

Keywords:
Quaternary ammonium salt
Bis(trifluoromethanesulfonyl)imide (TFSI)
Ionic liquids
Thermal analysis
X-ray diffraction
Physicochemical properties

ABSTRACT

Eight new monocationic quaternary ammonium (QA) salts with the bis(trifluoromethanesulfonyl)imide (TFSI) anion were prepared by metathesis using our previously reported QA halides as precursors. New salts were characterized both in liquid and solid state using ^{1}H and ^{13}C NMR techniques, mass spectroscopy and elemental analysis together with X-ray diffraction and thermoanalytical methods. In addition, residual water content, viscosity and conductivity measurements were made for three of the room-temperature ionic liquids (RTILs). The crystal structures of three compounds were determined by X-ray single crystal diffraction. Powder diffraction was used to study the crystallinity of the solid salts and to compare structural similarities between the single crystals and the microcrystalline bulk powders. Three of the salts are liquid below room temperature, having broad liquid ranges (~300 °C), and in total five out of eight salts melt below 100 °C. Moreover, powder diffraction data of the two RTILs were able to be measured at sub-ambient temperatures using *in situ* low-temperature powder X-ray diffraction revealing high crystallinity on both RTILs below their freezing point. The RTILs presented relatively high conductivities (~0.1–0.2 S m^{-1}) and moderate to relatively low viscosities. The determined physicochemical properties of the reported ILs suggest their applicability on various applications such as heat transfer fluids, high temperature synthesis and lubricants.

1. Introduction

Room-temperature ionic liquids (RTILs) have already been extensively studied by several authors due to their unique characteristics which have enabled their use in numerous applications [1–6]. Most of the previous studies still focus on costly imidazolium based ionic liquids to which ammonium and phosphonium based compounds are an alternative since they can be produced from readily available low cost materials [7–10]. Applications of ammonium-based ILs include their use as a reaction solvent [11,12] and a recent study indicates that certain ammonium-based ILs might possess anti-cancer activity [13]. Due to their wider electrochemical window and higher cathodic stability QA ILs are attractive alternatives to traditional aromatic ILs in electrochemical applications [14–17].

Introducing an oxygen-containing side chain has been proven to reduce the toxicity of certain ionic liquids [18,19] and it modifies their solvent properties and thermal behaviour. It also has a tendency to reduce the viscosity of QA-cation type ILs [20–26]. Moreover, ether-functionalized ILs have been proven to be more efficient in palladium-catalyzed Suzuki reactions than the non-substituted ones [27].

Building new types of ionic liquids with different functionalities prepares the way for a broader range of applications. The aim of our research in general is to develop new QA based salts that encompass ionic liquid nature – favorably having a broad liquid range, low viscosity, good electrochemical properties and low melting point combined with good thermal stability and desired solubility properties. This will be achieved by methods of crystal engineering: pairing systematically newly designed functionalized QA based cations with various anions, and performing systematic structural and thermoanalytical evaluations of the novel materials and exploring their physical properties. In our previous studies we have reported several series of QA salts with different counteranions [28–33]. In this study, some of the previously synthesized QA halides have been paired with the bis(trifluoromethanesulfonyl)imide as the melting point lowering effect of the TFSI anion is a well known fact. Because our study focuses on structural characterization and thermal analysis of the QA salts, the performed synthesis methods were not fully optimized, although majority of the salts were already afforded in moderate to good yields.

The ^{1}H and ^{13}C NMR spectroscopy, elemental analysis and ESI TOF MS measurements were used to verify chemical composition and purity of the compounds. The potential presence of residual

* Corresponding author. Fax: +358 14 2602501.
E-mail address: manu.k.lahtinen@jyu.fi (M. Lahtinen).

0022-2860/$ - see front matter © 2010 Elsevier B.V. All rights reserved.
doi:10.1016/j.molstruc.2010.08.036

bromide content in the TFSI salts were examined by inspecting corresponding mass regions of relevant mass spectra. X-ray powder diffraction was used to study the crystallinity of the salts and to compare structural properties between the single crystal structures and their powdery forms, when applicable. The thermal properties of the salts were examined by thermogravimetry (TG/DTA) and differential scanning calorimetry (DSC) and the effect of different anions to the characteristics of the salts were viewed by comparing these results. Viscosity and conductivity, as well as the UV–Vis spectra of the three room-temperature ionic liquids were obtained by capillary electrophoresis and their residual water content was determined with Karl Fischer titration. Densities for the fluid salts **5, 7** and **8** were determined using a pycnometer.

2. Experimental section

2.1. Synthesis and analysis

2.1.1. General procedure

All reagents were used as achieved from manufacturers. The precursors (QA halides) for compounds **1–8** (Scheme 1) were prepared as described in our previous studies [29–33].

The final TFSI salts were prepared by dissolving the QA halide in a minimum volume of water and adding the stoichiometric amount of lithium bis(trifluoromethanesulfonyl)-imide ($C_2F_6NO_4S_2Li$) dissolved in a minimum amount of water. The mixture was stirred overnight at room temperature. The product, QA TFSI, precipitated from the solution or formed a separate liquid layer. The raw product was filtered or decanted and washed with water until the $AgNO_3$-test was negative. If necessary, the product was recrystallized from an appropriate solvent, i.e. dichloromethane. The purified products were finally dried *in vacuo*.

2.1.2. (*1*) Dibenzyl dimethylammonium bis(trifluoromethylsulfonyl) imide

Reagents: dibenzyl dimethylammonium bromide (1.0 g, 3.2 mmol) and $C_2F_6NO_4S_2$ Li (0.84 g, 2.9 mmol). The yield (white powder) was 1.4 g (88%).

^{1}H NMR ($CDCl_3$, 400 MHz, ppm): 2.89 (6 H, s, N–C**H**$_3$), 4.54 (4 H, s, N–C**H**$_2$–), 7.44–7.51 (10 H, m, Ar-**H**). ^{13}C NMR ($CDCl_3$, 100 MHz, ppm): 48.35 (2 C, N–**C**H$_3$), 69.02 (2 C, N–**C**H$_2$–), 115.10, 118.30, 121.49, 124.67 (2 C, –**C**F$_3$), 126.39, 129.52, 131.17, 133.01 (12 C, Ar-**C**). ESI–TOF MS: *m*/*z* calculated for $C_{18}H_{20}N_2O_4S_2F_6$ [M-TFSI]$^+$: 226.16; found [M-TFSI]$^+$: 226.14. Elemental analysis: calculated for $C_{18}H_{20}N_2O_4S_2F_6$: C, 42.68; H, 3.98; N, 5.53. Found C, 42.63; H, 3.98; N, 5.58.

2.1.3. (*2*) Dimethyldi(3-methylbenzyl) ammonium bis(trifluoromethylsulfonyl)imide

Reagents: dimethyldi(3-methylbenzyl) ammonium chloride (1.0 g, 3.5 mmol) and $C_2F_6NO_4S_2$ Li (0.93 g, 3.2 mmol). The yield (white powder) was 1.8 g (95%).

^{1}H NMR ($CDCl_3$, 400 MHz, ppm): 2.37 (6 H, s, Ar-C**H**$_3$), 2.89 (6 H, s, N–C**H**$_3$), 4.48 (4 H, s, N–C**H**$_2$–), 7.24–7.34 (8 H, m, Ar-**H**). ^{13}C NMR ($CDCl_3$, 100 MHz, ppm): 21.15 (2 C, Ar-**C**H$_3$), 48.43 (2 C, N–**C**H$_3$), 69.07 (2 C, N–**C**H$_2$–), 115.12, 118.32, 121.51, 124.70 (2 C, –**C**F$_3$), 126.35, 129.30, 129.98, 131.86, 133.60, 139.58 (12 C, Ar-**C**). ESI–TOF MS: *m*/*z* calculated for $C_{20}H_{24}N_2O_4S_2F_6$ [M-TFSI]$^+$: 254.19; found [M-TFSI]$^+$: 254.16. Elemental analysis: calculated for $C_{20}H_{24}N_2O_4S_2F_6$: C, 44.94; H, 4.53; N, 5.24. Found C, 44.97; H, 4.67; N, 5.23.

2.1.4. (*3*) Dimethyldi(4-methylbenzyl) ammonium bis(trifluoro methylsulfonyl)imide

Reagents: dimethyldi(4-methylbenzyl) ammonium chloride (1.0 g, 3.5 mmol) and $C_2F_6NO_4S_2$ Li (1.11 g, 3.9 mmol). The yield (white powder) was 1.7 g (84%).

^{1}H NMR ($CDCl_3$, 400 MHz, ppm): 2.37 (6 H, s, Ar-C**H**$_3$), 2.85 (6 H, s, N–C**H**$_3$), 4.46 (4 H, s, N–C**H**$_2$–), 7.23–7.35 (8 H, m, Ar-**H**). ^{13}C NMR ($CDCl_3$, 100 MHz, ppm): 21.25 (2 C, Ar-**C**H$_3$), 48.12 (2 C, N–**C**H$_3$), 68.74 (2 C, N–**C**H$_2$–), 115.11, 118.31, 121.50, 123.40 (2 C, –**C**F$_3$), 123.23, 130.15, 132.86, 141.53 (12 C, Ar-**C**). ESI–TOF MS: *m*/*z* calculated for $C_{20}H_{24}N_2O_4S_2F_6$ [M-TFSI]$^+$: 254.19; found [M-TFSI]$^+$: 254.16. Elemental analysis: calculated for $C_{20}H_{24}N_2O_4S_2F_6$: C, 44.94; H, 4.53; N, 5.24. Found C, 45.00; H, 4.64; N, 5.20.

2.1.5. (*4*) Dimethyldi(4-methoxybenzyl) ammonium bis(trifluoromethylsulfonyl)imide

Reagents: dimethyldi(4-methoxybenzyl) ammonium bromide (1.0 g, 2.7 mmol) and $C_2F_6NO_4S_2$ Li (0.71 g, 2.5 mmol). The yield (white powder) was 1.5 g (99%).

^{1}H NMR ($CDCl_3$, 400 MHz, ppm): 2.82 (6 H, s, O–C**H**$_3$), 3.82 (6 H, s, N–C**H**$_3$), 4.44 (4 H, s, N–C**H**$_2$–), 6.93–7.39 (8 H, m, Ar-**H**). ^{13}C NMR ($CDCl_3$, 100 MHz, ppm): 47.77 (2 C, O–**C**H$_3$), 55.41 (2 C, N–**C**H$_3$), 68.48 (2 C, N–**C**H$_2$–), 114.85, 118.18, 134.38, 161.65 (12 C, Ar-**C**),

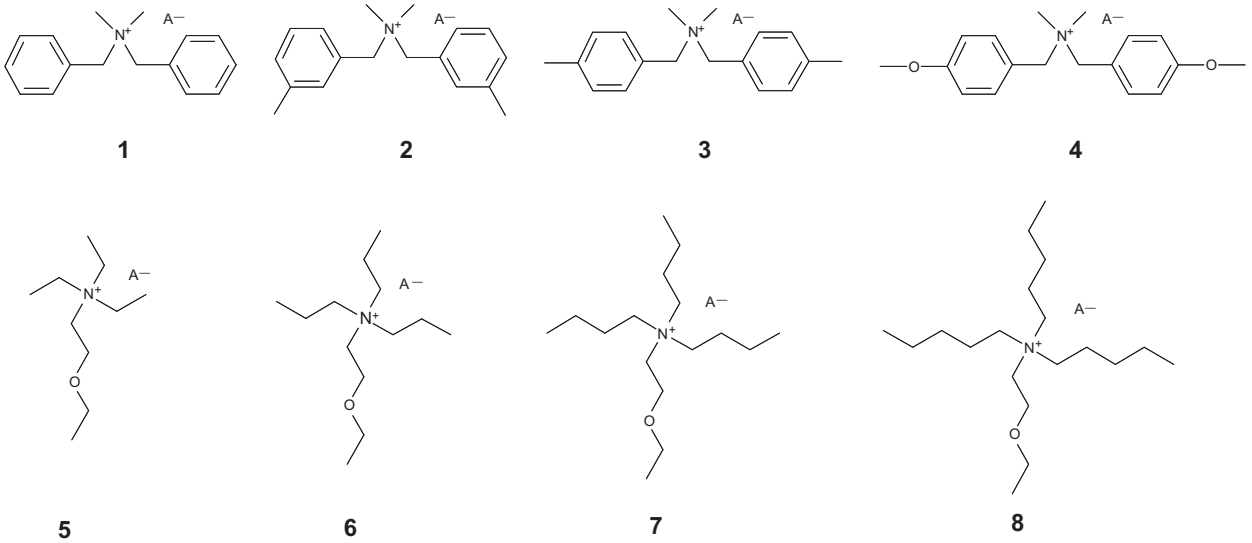

Scheme 1. Molecular structures of the compounds **1–8**. "A$^-$" represents the TFSI-anion.

115.14, 118.30, 121.50, 124.73 (2 C, –**C**F_3). ESI–TOF MS: *m*/*z* calculated for $C_{20}H_{24}N_2O_6S_2F_6$ $[M\text{-}TFSI]^+$: 286.18; found $[M\text{-}TFSI]^+$: 286.16. Elemental analysis: calculated for $C_{20}H_{24}N_2O_6S_2F_6$: C, 42.40; H, 4.27; N, 4.96. Found C, 42.63; H, 4.30; N, 4.80.

*2.1.6. (**5**) Triethyl ethoxyethyl ammonium bis(trifluoro methylsulfonyl)imide*

Reagents: triethyl ethoxyethyl ammonium bromide (2.0 g, 6.8 mmol) and $C_2F_6NO_4S_2$ Li (2.03 g, 7.1 mmol). The yield (colourless liquid) was 2.6 g (84%).

^{1}H NMR ($CDCl_3$, 400 MHz, ppm): 1.18 (3 H, t, O–CH_2–C**H**$_3$), 1.31 (9 H, t, N–CH_2–C**H**$_3$), 3.35 (6 H, q, N–C**H**$_2$–CH_3), 3.39–3.42 (2 H, m, N–C**H**$_2$–CH_2–O), 3.51 (2 H, q, O–C**H**$_2$–CH_3), 3.75–3.76 (2 H, m, N–CH_2–C**H**$_2$–O). ^{13}C NMR ($CDCl_3$, 100 MHz, ppm): 7.41 (3 C, N–CH_2–**C**H_3), 14.72 (1 C, O–CH_2–**C**H_3), 53.95 (3 C, N–**C**H_2–CH_3), 56.87 (1 C, N–**C**H_2–CH_2–O), 63.42 (1 C, N–CH_2–**C**H_2–O), 67.11 (1 C, O–**C**H_2–CH_3), 115.07, 118.27, 121.46, 124.65 (2 C, –**C**F_3). ESI–TOF MS: *m*/*z* calculated for $C_{12}H_{24}N_2O_5S_2F$ $[M\text{-}TFSI]^+$: 174.19; found $[M\text{-}TFSI]^+$: 174.15. Elemental analysis: calculated for $C_{12}H_{24}N_2O_5S_2F_6$: C, 31.71; H, 5.32; N, 6.16. Found C, 31.52; H, 5.22; N, 6.29.

*2.1.7. (**6**) Tripropyl ethoxyethyl ammonium bis(trifluoromethylsulfo nyl)imide*

Reagents: tripropyl ethoxyethyl ammonium bromide (1.0 g, 3.0 mmol) and $C_2F_6NO_4S_2$ Li (0.87 g, 3.0 mmol). The yield (yellow powder) was 1.2 g (80%).

^{1}H NMR ($CDCl_3$, 400 MHz, ppm): 1.01 (9 H, t, N–CH_2–CH_2–C**H**$_3$), 1.20 (3 H, t, O–CH_2–C**H**$_3$), 1.68–1.74 (6 H, m, N–CH_2–C**H**$_2$–CH_3), 3.18–3.23 (6 H, m, N–C**H**$_2$–CH_2–CH_3), 3.50–3.53 (4 H, m, N–C**H**$_2$–CH_2–O–C**H**$_2$–CH_3), 3.78 (2 H, m, N–CH_2–C**H**$_2$–O).

^{13}C NMR ($CDCl_3$, 100 MHz, ppm): 10.44 (3 C, N–CH_2–CH_2–**C**H_3), 14.87 (1 C, O–CH_2–**C**H_3), 15.54 (3 C, N–CH_2–**C**H_2–CH_3), 58.63, 67.21 (2 C, N–**C**H_2–CH_2–O–**C**H_2–CH_3), 61.23 (3 C, N–**C**H_2–CH_2–O), 63.66 (1 C, –C**H**$_2$–O–CH_2–) 115.10, 118.29, 121.49, 124.68 (2 C, –**C**F_3). ESI–TOF MS: m/z calculated for $C_{15}H_{30}N_2O_5S_2F_6$ $[M\text{-}TFSI]^+$: 216.23; found $[M\text{-}TFSI]^+$: 216.23. Elemental analysis: calculated for $C_{15}H_{30}N_2O_5S_2F_6$: C, 36.28; H, 6.09; N, 5.64. Found C, 35.95; H, 6.11; N, 5.65.

*2.1.8. (**7**) Tributyl ethoxyethyl ammonium bis(trifluoromethylsulfonyl) imide*

Reagents: tributyl ethoxyethyl ammonium bromide (1.0 g, 2.9 mmol) and $C_2F_6NO_4S_2$ Li (0.76 g, 2.6 mmol). The yield (yellow liquid) was 1.5 g (96%).

^{1}H NMR ($CDCl_3$, 400 MHz, ppm): 0.99 (9 H, t, –CH_2–CH_2–C**H**$_3$), 1.18 (3 H, t, O–CH_2–C**H**$_3$), 1.36–1.44 (6 H, m, –CH_2–C**H**$_2$–CH_3), 1.58–1.66 (6 H, m, –C**H**$_2$–CH_2–CH_3), 3.20–3.25 (6 H, m, N–C**H**$_2$–CH_2–CH_2–), 3.48–3.53 (4 H, m, N–C**H**$_2$–CH_2–O–C**H**$_2$–CH_3), 3.75 (2 H, m, N–CH_2–C**H**$_2$–O–). ^{13}C NMR ($CDCl_3$, 100 MHz, ppm): 13.39 (3 C, –CH_2–CH_2–**C**H_3), 14.81 (1 C, O–CH_2–**C**H_3), 19.48 (3 C, –CH_2–**C**H_2–CH_3), 23.78 (3 C, –**C**H_2–CH_2–CH_3), 58.41 (1 C, N–**C**H_2–CH_2–O), 61.23 (3 C, N–**C**H_2–CH_2–CH_2–),63.68 (1 C, N–CH_2–**C**H_2–O–), 67.16 (1 C, O–**C**H_2–CH_3), 115.07, 118.29, 121.48, 124.68 (2 C, –**C**F_3). ESI–TOF MS: *m*/*z* calculated for $C_{18}H_{36}N_2O_5S_2F_6$ $[M\text{-}TFSI]^+$: 258.28; found $[M\text{-}TFSI]^+$: 258.27. Elemental analysis: calculated for $C_{18}H_{36}N_2O_5S_2F_6$: C, 40.14; H, 6.74; N, 5.20. Found C, 39.75; H, 6.55; N, 5.50.

*2.1.9. (**8**) Tripentyl ethoxyethyl ammonium bis(trifluoromethyl sulfonyl)imide*

Reagents: tripentyl ethoxyethyl ammonium bromide (1.0 g, 2.6 mmol) and $C_2F_6NO_4S_2$ Li (0.68 g, 2.4 mmol). The yield (yellow liquid) was 1.3 g (86%).

^{1}H NMR ($CDCl_3$, 400 MHz, ppm): 0.94 (9 H, t, –CH_2–CH_2–C**H**$_3$), 1.21 (3 H, t, O–CH_2–C**H**$_3$), 1.34–1.43 (12 H, m, –C**H**$_2$–C**H**$_2$–CH_3), 1.63–1.69 (6 H, m, N–CH_2–C**H**$_2$–), 3.21–3.25 (6 H, m, N–C**H**$_2$–CH_2–CH_2–), 3.50–3.54 (4 H, m, N–C**H**$_2$–CH_2–O–C**H**$_2$–CH_3), 3.77 (2 H, m, N–CH_2–C**H**$_2$–O–). ^{13}C NMR ($CDCl_3$, 100 MHz, ppm): 13.63 (3 C, –CH_2–CH_2–**C**H_3), 14.81 (1 C, O–CH_2–**C**H_3), 21.53 (3 C, N–CH_2–**C**H_2–CH_2), 22.00, 28.13 (6 C, –**C**H_2–**C**H_2–CH_3), 58.38, 67.15 (2 C, N–**C**H_2–CH_2–O–**C**H_2), 59.63 (3 C, N–**C**H_2–CH_2–O), 67.15 (1 C, N–CH_2–**C**H_2–O–), 115.07, 118.27, 121.46, 124.66 (2 C, –**C**F_3). ESI–TOF MS: *m*/*z* calculated for $C_{21}H_{42}N_2O_5S_2F_6$ $[M\text{-}TFSI]^+$: 300.33; found $[M\text{-}TFSI]^+$: 300.28. Elemental analysis: calculated for $C_{21}H_{42}N_2O_5S_2F_6$: C, 43.44; H, 7.29; N, 4.82. Found C, 42.65; H, 7.16; N, 5.05.

2.2. Characterization in the liquid state

The formation of the desired salts was confirmed by ^{1}H and ^{13}C NMR spectroscopy and ESI TOF mass spectroscopy and elemental analysis was used to verify the purity of the salts. ^{1}H and ^{13}C NMR spectra were measured in $CDCl_3$ (or appropriate solvent) at 30 °C by using a Bruker Avance DRX 400 NMR spectrometer operating at 400 MHz for ^{1}H and at 100 MHz for ^{13}C. Mass spectra were obtained by using the Micromass LCT time of flight (TOF) mass spectrometer with electrospray ionization (ESI). The measurements were made using the positive ion mode with a sample concentration of 25 mg/l in a methanol solution. The elemental analyses were carried out with Vario EL III CHN elemental analyzer using sample weights of 2–8 mg. For salts **5, 7** and **8**, the residual water contents were measured with Mettler Toledo C30 Coulometric Karl-Fischer titrator and densities were determined using a 5 ml capillary pycnometer.

Temperature dependent dynamic viscosities of **5**, **7** and **8** were measured with Brookfield DV-III rheometer using conical geometry (CPE-51 spindle) at temperatures 25–60 °C with a Brookfield TC-500 water circulator. The sample volume was 0.5 ml. UV–Vis spectra, viscosities of IL/molecular solvent mixtures and conductivity measurements were performed with a HP CE^{3D} G1600 AX apparatus (Agilent, Waldbronn, Germany) equipped with a diode array detector (DAD) and an air cooling unit for the capillary. More detailed descriptions of the measurements including calibration data can be found in the Supplementary material.

2.3. X-ray single crystal diffraction structures

The crystal structures for compounds **2**, **3** and **4** were determined by X-ray single crystal diffraction. Colourless single crystals were obtained by diffusion crystallization from suitable solvent, i.e. mixture of methanol and diethyl ether or mixture of ethanol and pentane.

The crystallographic data were recorded with a Kappa APEX II diffractometer at −120 °C using graphite monochromatized Mo Kα (λ = 0.71073 Å) radiation. The data were processed with DenzoSMN v0.95.373 [34,35] and the absorption corrections were performed using SADABS2008 [36]. The structures were solved by using direct methods (SHELXS-97 [37] or SIR2004 [38] and refined on F^2 by full matrix least squares techniques (SHELXL-97 [39]) by using anisotropic displacement parameters for all non-hydrogen atoms. Hydrogen atoms, except those of solvents, were calculated to their positions as riding atoms by using isotropic displacement parameters. The isotropic displacement parameters were fixed to be 1.2–1.5 times larger than those of the attached host atom. The programs Diamond [40] and Mercury [41] were used for depicting the crystal structures.

2.4. X-ray powder diffraction analyses

The X-ray powder diffraction data was measured with PANalytical X'Pert PRO diffractometer in Bragg–Brentano geometry using step-scan technique, and Johansson monochromator to produce pure Cu $K\alpha_1$ radiation (1.5406 Å; 45 kV, 30 mA). Hand ground

powder samples were prepared either on standard steel plate holders (having 10 or 16 mm diameter sample cavity) or on a silicon-made zero-background holder (petrolatum jelly was used as an adhesive). The data was collected by X'Celerator detector using continuous scanning mode in 2θ-range of 4–70° with a step size of 0.017° and sample dependently counting time of 40–100 s per step. Programmable divergence slit (PDS) was used to set irradiated length on sample to 10 mm together with 10 or 15 mm incident beam mask. Soller slits of 0.02° rad were used both on incident and diffracted beam side together with anti-scatter slits 4° and 13 mm (4° and 6.6 mm for non-ambient measurements), respectively.

For *in situ* low-temperature measurements, the default sample stage was changed to an Anton Paar TTK 450 low-temperature chamber with automated height-controller of the stage. Vacuum pump system and liquid N_2 cooling unit were used to control measuring conditions. The sample was prepared on a sample cavity inside a TTK 450 chamber and cooled under vacuum (0.129 mbar) from 25 to −110 °C with a cooling rate of 10 °C/min by controlled liquid nitrogen cooling. And then heated at a rate of 10 °C/min to selected measurement temperatures such as −30 and −110 °C, at which diffraction patterns were recorded isothermically.

All diffraction data was converted from automatic slit mode (ADS) to a fixed slit mode (FDS) data in X'Pert HighScore Plus v. 2.2d software package before further analyses. The simulated powder diffraction patterns were calculated by the program Mercury [41] from the CIFs of the QA salts under investigation.

2.5. Thermal properties

The thermal transitions of the QA salts were examined on a power compensation type Perkin Elmer Diamond DSC. Measurements were carried out under nitrogen atmosphere (flow rate 50 ml/min) using 50 µl sealed aluminum pans. To ensure good thermal contact between a sample and a pan and to minimize the free volume inside the pan, the sealing was made using a 30 µl aluminum pan with pinholes. The temperature and energy calibration was made using In metal standard (156.6 °C; 28.45 J/g). The samples were heated at a rate of 5–10 °C/min either from −60 °C or −50 °C to a temperature close to the observed decomposition temperature of each salt and then cooled down to the starting temperature at a rate of 5 °C/min. The cycle was repeated twice and the sample weights used were about 2–20 mg. The extreme low temperature DSC-scans were made using a Mettler Toledo DSC829 DSC. The samples were heated under nitrogen atmosphere (50 ml/min) at a rate of 10 °C/min from −120 °C to 50 °C and cooled back to −120 °C at a rate of 5 °C/min. The cycle was repeated twice. The sample pans were cold pressed and holes were punctured into the lid to release any forming pressure, sample weights of 5–10 mg were used. The calibration of the instrument was made using hexane, water, indium and zinc.

The thermal decomposition paths for compounds **1**–**8** were obtained with PerkinElmer TGA 7 thermogravimetric analyzer. Measurements were carried out in open platinum pan under air atmosphere (flow rate of 50 ml/min) with heating rate of 5 °C/min on temperature range of 25–900 °C. The temperature calibration of the analyzer was made using Curie-point calibration technique (Alumel, Ni, Perkalloy, Fe). The weight balance was calibrated by measuring the standard weight of 50 mg at room temperature. The sample weights used in the measurements were about 5–20 mg.

3. Results and discussion

3.1. Characterization in liquid and solid state

According to the ^1H, ^{13}C NMR spectra and mass spectra the salts were free of solvents and any other impurities. The absence of the bromide-ion was confirmed by the mass spectra. The residual water content of RTILs **5, 7** and **8** was found to be <150 ppm after drying *in vacuo*.

The temperature dependent dynamic viscosities of TFSI salts **5, 7** and **8** were made by rheometer and the results are presented in Fig. 1. In the literature the viscosities of aliphatic monocationic ammonium-based ILs with the TFSI anion have been reported to vary between 50 and 200 mPa s at 25 °C [6]. Compared to those, viscosities of these new ILs fall in the same category being 70 mPa s, 315 mPa s and 312 mPa s, respectively. At 60 °C the viscosities drop to 18 mPa s, 43 mPa s and 48 mPa s. The densities of compounds **5, 7** and **8** at room temperature were 1.36 g cm^{-3}, 1.23 g cm^{-3} and 1.19 g cm^{-3}, respectively.

Glass-forming liquids can be classified as either "strong" or "fragile", depending on their behaviour [42]. One approach to study this property is by using the so called Angell plot, log η vs. glass transition scaled temperature, T_g/T (Fig. 2). Liquids falling on the right hand side of the plot, showing the largest deviation from the Arrhenius behaviour, are considered as fragile. In the Fig. 2 the unit Poise is used instead of the standard mPa s to facilitate comparisons to ILs found in the literature [43–48]. When compared to other ILs the fragilities of these new compounds are similar being rather fragile and therefore the properties have strong temperature dependence near the T_g. Comparing the two new salts, differences in their behaviour are very small which could be expected since the compounds are very similar.

In addition, the fluidities (η^{-1}, η is viscosity) of compounds **5**, **7** and **8** were studied using Arrhenius plots (Fig. 3). To elucidate the fluidity over longer liquid range the glass transition temperature is included in the second plot (salts **5** and **8**). At the glass transition temperature, the value of fluidity is approximated to be 10^{11} [49].

Conductivity measurements were performed on RTILs **5**, **7** and **8** using capillary electrophoresis. Details can be found in the electronic supplementary information (ESI), as well as the UV–Vis spectra and the parallel viscosity measurements using electrophoresis instead of rheometer. The conductivities of pure ILs were κ = 0.26 S m^{-1}, κ = 0.14 S m^{-1} κ = 0.11 S m^{-1} for **5**, **7** and **8**, respectively. The conductivities could be noticeably increased (κ = 0.90–2.14 S m^{-1}) by using IL-methanol mixtures in the solvent molar fraction range of 0.89–0.97 (see ESI). Determined values are lower than that of traditional conductive solvents but fall into the same range with some previously reported similar monocationic QA ILs [6].

Moreover, combining the data from viscosity, conductivity and density measurements we find the molar conductivities of these

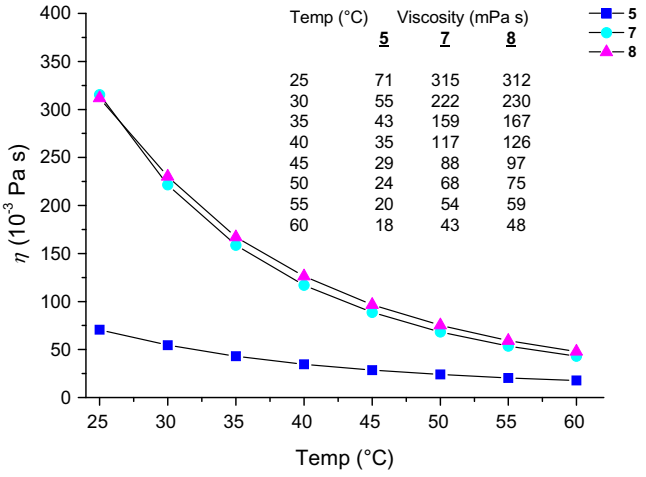

Fig. 1. Temperature dependent viscosities of **5**, **7** and **8** obtained by rheometer.

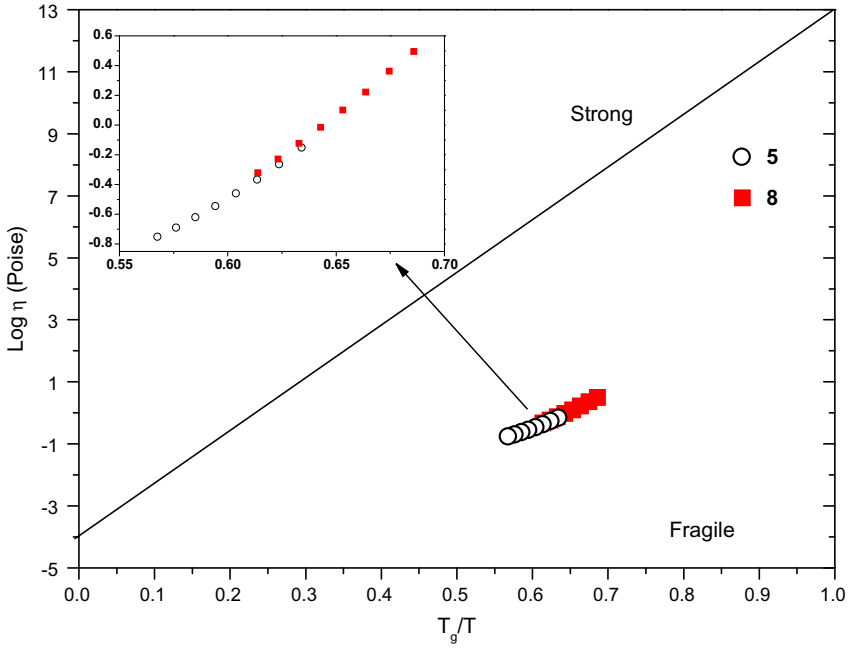

Fig. 2. Angell plot of ionic liquids **5** and **8**.

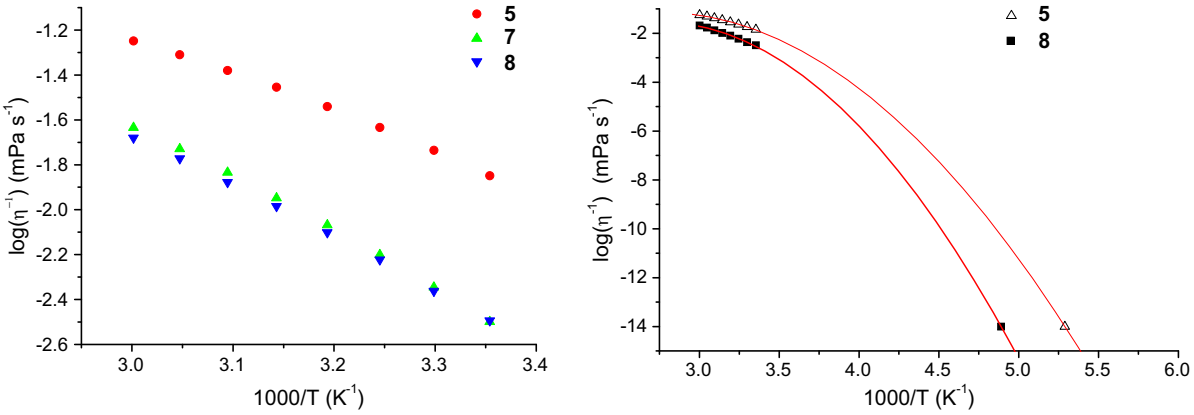

Fig. 3. Left: Arrhenius plots of fluidities of salts **5**, **7** and **8**. Right: Arrhenius plot of the fluidities of **5** and **8** including the values in glass transition temperature.

compounds to be 0.87 S cm^2 mol^{-1}, 0.61 S cm^2 mol^{-1} and 0.54 S cm^2 mol^{-1}, and the Walden products 60.8 S Pa s cm^2 mol^{-1}, 193.1 S Pa s cm^2 mol^{-1} and 167.5 S Pa s cm^2 mol^{-1}, respectively. Compared to previously reported QA ILs [6] the molar conductivities for all three ILs are similar. The Walden product for compound **5** is again similar to previously reported, but for compounds **7** and **8** the values are noticeably higher, due to higher viscosities.

3.2. X-ray single crystal diffraction structure analysis

The crystallographic data of compounds **2**, **3** and **4** are presented in Table 1 and the selected bond angles and distances in Table 2. The solidified salts other than above did either not form single crystals in re-crystallization or the quality of the crystals was inadequate for structure determination.

Compound **2** crystallizes in a monoclinic space group $P2_1/n$ with one cation and one anion in the asymmetric unit being structurally similar to the analogous chloride salt [33]. Cation appears in a W-conformation whereas the anion appears in *trans*-conformation having the trifluoromethyl groups on the opposite sides of the imide core (Fig. 4). The packing is affected by Coulombic interactions as well as several weak hydrogen–fluorine interactions (C–H···F < 2.66 Å) (Fig. 5a). Each cation is connected to three different anions by these contacts and the hydrogen to fluorine distances vary from 2.60 to 2.65 Å with bond angles from 123° to 134°, respectively. The shortest distance between nitrogen and fluorine is 4.38(3) Å and between cation nitrogen and anion nitrogen atoms is 4.45(5) Å. Cations are also packed via intermolecular methyl C–H-π and face to face π–π interactions between the substituted phenyl groups as can be seen in Fig. 5b. The cations form pairs via C–H-π interactions arranging in layers along the crystallographic *a*-axis. These pairs then form infinite chains via face to face π–π interactions. Similarly the anions are packed in "planar" zigzag chains along the (−1 0 1) plane.

Compound **3** crystallizes in triclinic spacegroup *P*-1 having one cation and a disordered anion in the asymmetric unit (Fig. 6). Again, the cations appear in W-conformation and the anions are in *trans*-conformation as in the structure **2**. The cation is connected to one anion with a weak C–H···F interaction (<2.61 Å) with bong angle of 145°. The cation also has weak C–H···O interactions between six anions, one of which is bifurcated. The lengths of these interactions vary from 2.34 to 2.68 Å with bond angles of

Table 1
Crystallographic data for compounds **2**, **3** and **4**.

Compound	**2**	**3**	**4**
Formula	$C_{20}H_{24}F_6N_2O_4S_2$	$C_{20}H_{24}F_6N_2O_4S_2$	$C_{20}H_{24}F_6N_2O_6S_2$
M_r (g/mol)	543.53	534.53	566.53
Crystal system	Monoclinic	Triclinic	Orthorhombic
Space group	$P2_1/n$ (No. 14)	P-1 (No. 2)	$P2_12_12_1$ (No. 19)
a (Å)	12.078(2)	8.7581(4)	14.204(3)
b (Å)	15.200(3)	9.0398(7)	17.094(3)
c (Å)	13.338(3)	16.4596(7)	20.323(4)
α (°)	90	100.897(2)	90
β (°)	103.85(3)	96.011(3)	90
γ (°)	90	110.487(2)	90
V (Å^3)	2377.6(8)	1177.83(12)	4934.5(17)
Z	4	2	8
ρ_{calcd} (g/cm^3)	1.493	1.507	1.525
μ (mm^{-1})	0.301	0.303	0.300
F (0 0 0)	1104	552	2336
Crystal size (mm^3)	0.2 × 0.2 × 0.3	0.08 × 0.3 × 0.4	0.3 × 0.3 × 0.36
θ range (°)	2.04–28.46	2.53–25	2.74–28.78
Reflections collected	30,067	15,101	37,756
Independent reflections	5959	4134	12,368
Data/restraints/parameters	5959/0/307	4134/0/313	12,368/0/649
GooF	1.096	1.062	1.010
R (int)	0.0637	0.0643	0.0516
Final R indices [$I > 2\sigma(I)$]	R_1 = 0.0665	R_1 = 0.1039	R_1 = 0.0533
	wR^2 = 0.1590	wR^2 = 0.3073	wR^2 = 0.0914
R indices (all data)	R_1 = 0.1028	R_1 = 0.1240	R_1 = 0.0847
	wR^2 = 0.1801	wR^2 = 0.3189	wR^2 = 0.1015
Largest diff. peak/hole (e/Å^3)	0.38 and −0.39	1.57–0.58	0.37 and −0.30
Flack parameter	–	–	0.114(51)

Table 2
Selected bond lengths (Å) and bond angles (°) with e.s.d.s for salts **2**, **3** and **4**.

Compound	**2**	**3**	**4**
N(1)–C(11)	1.496(4)	1.527(9)	1.532(4)
N(1)–C(21)	1.501(4)	1.537(9)	1.526(4)
N(1)–C(31)	1.531(4)	1.492(9)	1.497(3)
N(1)–C(41)	1.533(4)	1.506(9)	1.494(3)
C(11)–N(1)–C(21)	109.4(2)	107.0(5)	105.8(2)
C(11)–N(1)–C(31)	109.6(2)	110.3(6)	110.5(2)
C(11)–N(1)–C(41)	110.8(2)	110.1(6)	109.9(2)
C(21)–N(1)–C(31)	110.65(2)	110.7(6)	110.9(2)
C(21)–N(1)–C(41)	109.5(2)	109.6(6)	110.4(2)
C(31)–N(1)–C(41)	106.8(2)	109.1(5)	109.2(2)

136–172°, respectively. The shortest distance between cation nitrogen and anion nitrogen atoms is 3.99(2) Å. Along with Coulombic interactions the cations are packed via face to face π–π interactions between the substituted phenyl groups as can be seen in Fig. 7. The cations then form infinite chains along the crystallographic c-axis via face to face π–π interactions. The residual electron density with highest peak 1.57 e Å^{-3} is caused by the disordered anion. However, the observed disorder was too severe to be modelled properly around the defined anion coordinates but it is clearly caused by anion packing in helical chains in tunnel like loose void along c-axis (Fig. 7), so that the trifluoromethyl groups of the adjacent anions are against each other. Slight positional variation of these chains in the crystal lattice causes the observed residual density around the anion.

Compound **4** crystallizes in orthorhombic space group $P2_12_12_1$ having two cations and two anions in the asymmetric unit (Fig. 8). The structure is analogous with the corresponding bromide [29]. The cations yet again appear in W-conformation, the two cations mainly differing by the orientation of the methoxy groups

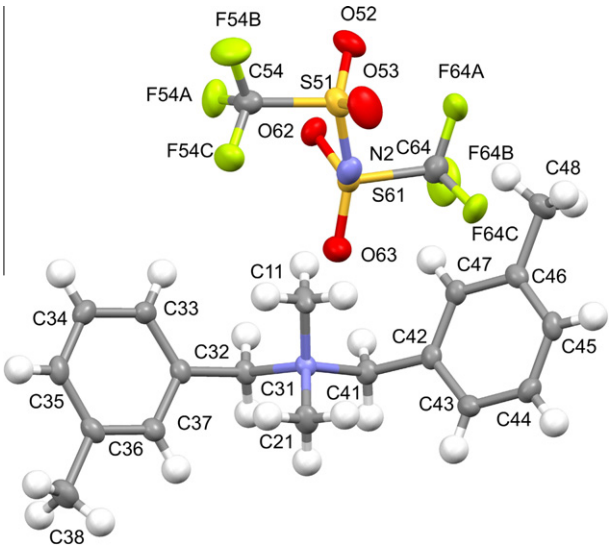

Fig. 4. The molecular structure and labelling scheme of compound **2**.

being pointing either to the same side or on opposite sides of the cation. The anions are in *trans*-conformation as in the structure **2** also forming helical chains (Fig. 9a). The packing is affected by Coulombic interactions and also by several weak interactions. Each cation is connected to one anion with a weak C–H···F interaction (<2.67 Å) with bong angles of 120° and 127°, respectively. Weak C–H···O interactions between two cations and eight anions also exist, some of which are bifurcated. The length of these interactions varies from 2.38 to 2.66 Å with bond angles of 129–170°, respectively. The shortest distance between cation nitrogen and anion nitrogen atoms is 4.01(3) Å. Cations are also packed via intermolecular face to face π–π interactions between the substituted phenyl groups as can be seen in Fig. 9b.

3.3. X–ray powder diffraction analysis

The powder X-ray diffraction (PXRD) patterns for compounds **2**, **3** and **4** are presented in Fig. 10 together with the simulated patterns from the corresponding single crystal structures. For salts **2** and **3**, the similarity between the bulk powder and the single crystal structure is obvious. Whereas on compound **4** few unidentified peaks for example at 10.5°, 11.7°, 12.1°, 13.1°, 14.7°, 15.9° and 21.0° in 2θ can be seen. These peaks indicate presence of either a polymorph or a hydrated form, from which the polymorph is the most likely candidate (see thermal analysis part). Compounds **1** and **6** are also crystalline (see ESI, Fig. S4) but did not produce any good quality single crystals suitable for structure determination.

To get further insight of the structural properties on the RTILs **5** and **7**, powder diffraction patterns were measured also at sub-ambient temperatures; −30 and −110 °C for **5** and −30 °C for **7** (compound **8** was not measured since it formed only a glassy solid). As tentatively suggested by the sharp melting/crystallization transitions obtained with DSC, both ILs proved to be highly crystalline in the solid phase. The powder diffraction patterns along with the corresponding DSC-scans are presented in Figs. 11 and 12, respectively. Salt **5** is completely amorphous at −110 °C whereas highly crystalline above cold crystallization that occurs about at −30 °C then melting sharply at −1.6 °C. In case of **7**, diffraction pattern have been presented using square rooted y-axis due to dramatic preferred orientation effect that can be observed on diffraction peaks 8.2° and 16.5° 2θ. The visual inspection of the sample while in the chamber revealed that the preferred orientation is induced by diffraction occurring from a highly oriented film-surface instead

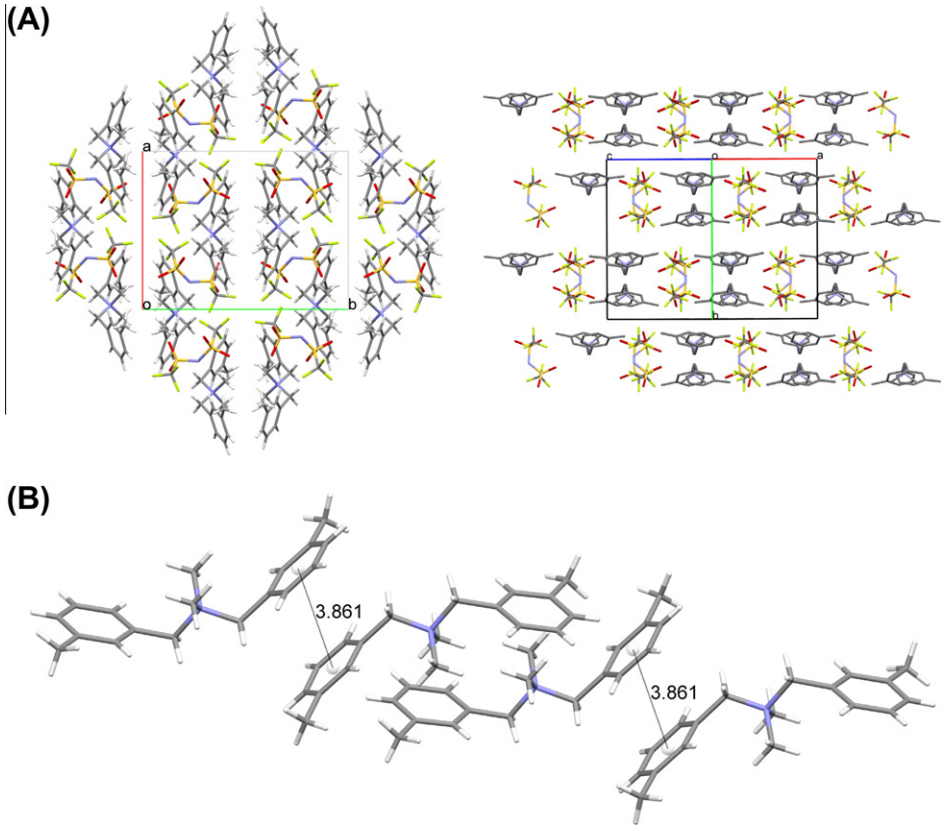

Fig. 5. (A) The packing of compound **2** left: viewed along the crystallographic *c*–axis. Right: along the (−1 0 1) plane (B) C–H-π and face to face π–π interactions forming the network of connections between cations. The anions have been removed for clarity.

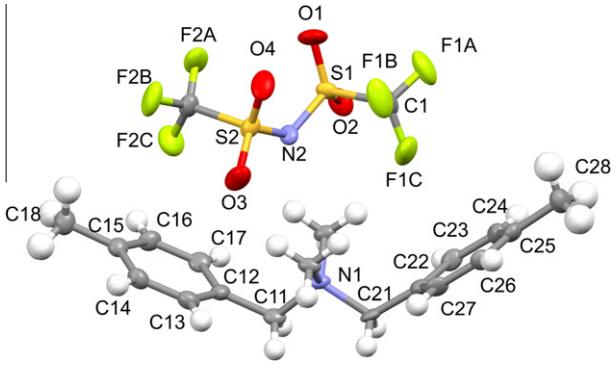

Fig. 6. The molecular structure and labelling scheme of compound **3**.

of a powder, as sample resided in the sample cavity in a form of transparent coating. Similar transparent coat-formation was observed also for **5**, but diffraction peaks are clearly less affected by crystal orientation effects. Diffraction patterns were used to investigate whether the low-temperature powder structures could be determined for **5** and **7**. In case of **5** first 19 diffraction peak positions were used as an input for the auto-indexing procedure made by DICVOL04 [50]. All the peaks can repeatedly be indexed by triclinic unit cell setting $a = 9.2376(21)$ Å, $b = 8.4410(39)$ Å, $c = 13.9017(69)$ Å, $\alpha = 84.833(29)°$, $\beta = 92.900(32)°$, $\gamma = 103.945(29)°$ and $V = 1047.28$ Å^3 with reasonably high figure of merits ($M_{19} = 43.1$, $F_{19} = 125.8$ (0.0058, 26)) [51]. Similar unit cell settings were acquired also by comparative auto-indexing in X'pert High-Score Plus. The given unit cell dimension could adequately be filled by two ion pair units of **5** (2 × (27 non-hydrogen atoms × 20 Å^3 space reserved for each atom including some space for hydrogen atom) addressing also potential correctness of the found unit cell The final unit cell refinement resulted good Pawley fit indicating correctness of the determined cell settings and space group *P*-1 (Pawley $\chi^2 = 4.52\%$, $R_{wp} = 0.15$ with 403 reflections). The structure determination was attempted by DASH [52] program that is based on simulated annealing method in which known structure moiety/moieties are needed to structure determination. The needed structure moieties for a cation and an anion was retrieved from the known structures and introduced to the DASH program. Unfortunately the data quality of the low-temperature diffraction pattern was still inadequate for successful structure determination as only the spatial position of the anion was able to be found whereas the position of the cation remained ambiguous. In case of compound **7**, few tentative monoclinic and orthorhombic unit cell settings were obtained but structure determination attempts failed on each time with tested cell and space group settings.

3.4. Thermal properties

The summarized results of the DSC measurements together with the decomposition temperatures obtained by TG/DTA are presented in Table 3. The examples of the DSC-scans are in Fig. 12 (see ESI for DSCs) and TG curves for all compounds are presented in Fig. 13. To emphasize the crystallization properties of the salts when they are cooled from a liquid state and then reheated, results of the second heating scans are also included in the Table 3. Many of the ILs, including one salt reported in this study, can form glassy states via a supercooled liquid state and thus can be cooled down below expected freezing point without initiation of crystallization [53]. Some of the ILs in glassy state can be recrystallized via a cold crystallization when heated above the glass transition

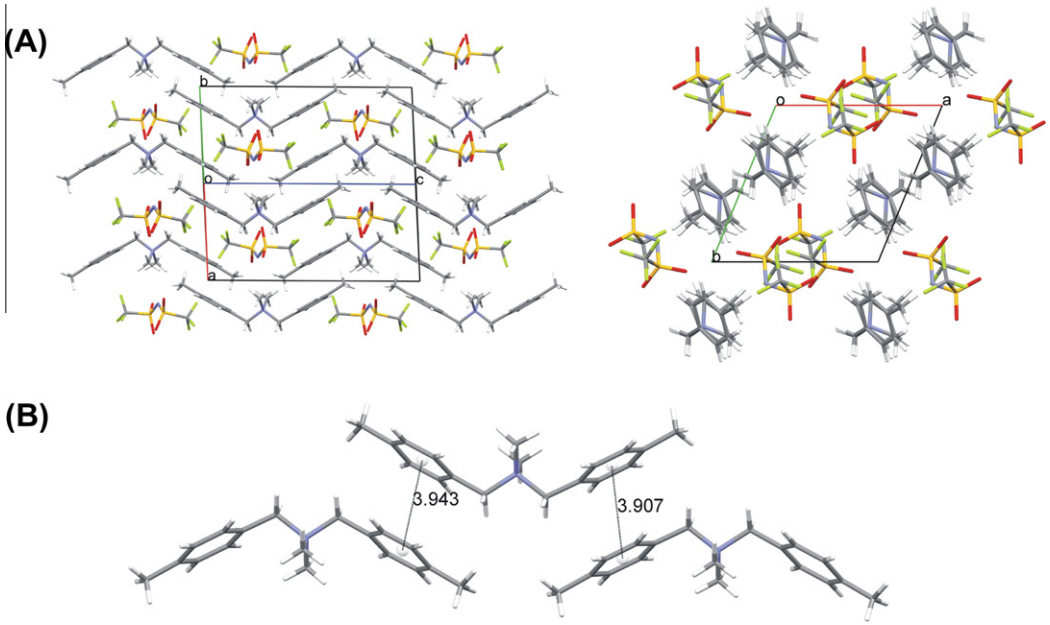

Fig. 7. (A) The packing of compound **3** left: along (1 −1 0) plane, right: along *c*-axis and (B) face to face π–π interactions forming the network of connections between cations. The anions have been removed for clarity.

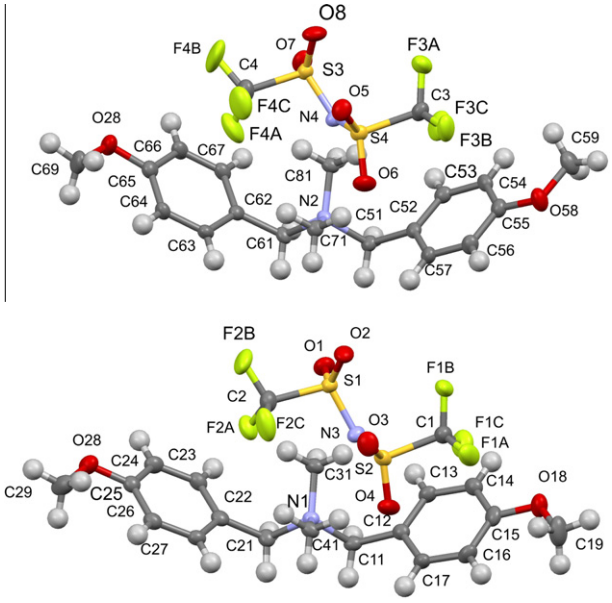

Fig. 8. The molecular structure and labelling scheme of compound **4**.

temperature, whereas certain salts will enter to a supercooled liquid state and simply form new glassy state when cooled again below the glass forming temperature.

All salts except **8** exhibit a melting transition on both heating scans. The aromatic salts (**1**–**4**) have melting points between 79 and 105 °C and the $RR'_3N^+A^-$ salts between <−60 and 62 °C.

The thermal behaviour of the compounds, apart from compound **8**, can roughly be divided in two groups. The first group is formed by salts **1**, **3**, **6** and **7**. They crystallize from a melt on cooling and re-melt on the second heating (Table 3). Both the melting points and their enthalpies observed on the second heating correspond well with those found on the first heating indicating good re-crystallization properties to form a same structural form with equal crystallinity from a melted state. Compound **2** behaves correspondingly but the re-crystallization on subsequent scans is incomplete which can be seen from the magnitude of melting enthalpy. Compounds of the second group, salts **4** and **5**, supercool on cooling and turn into a glass via glass transitions at low temperature. However, on reheating a cold crystallization occurs above the glass transition, followed by re-melting at temperature similar to that observed on the first heating scan. The re-crystallization of compound **4** on subsequent scans is incomplete and the presence of minor fraction of one or several polymorphs can be found in the DSC-scan. Salt **5** also exhibits polymorphism depending on the cooling rate (see ESI Fig. S7 for additional DSC-scans). Compound **8** is liquid at and below room temperature having a liquid range of 347 °C. By cooling it turns into glass but shows no other transitions. In all, five compounds **2**, **5**–**8**, are liquid below 100 °C and two salts somewhat above that.

The thermal decomposition of compounds **1–8** occur in one stage without identifiable cleavages. The decomposition of the aromatic compounds (**1**–**4**) starts at temperatures 244–306 °C and of the $RR'_3N^+A^-$ compounds (**5**–**8**) at 279–320 °C. Compared to the previously published analogous compounds with different anions the thermal stability is significantly increased. Only the PF_6^- anion results in similar thermal stabilities, but compounds with the TFSI anion also exhibit lower melting points [29–31,33].

4. Conclusions

Eight new small low melting point quaternary ammonium salts having TFSI as an anionic part were synthesized and characterized both in liquid and solid state. Together with determining various physicochemical properties of these salts, single crystal structures of three salts were determined. Five out of eight salts melt below 100 °C whereas three of the salts are fluid at room temperature. Viscosities of **5**, **7** and **8** at room temperature are 70 mPa s, 315 mPa s and 312 mPa s, respectively and decrease rapidly with increase of temperature being below 50 mPa s already at 60 °C. These salts also exhibit rather good conductivities (0.1–0.2 S m^{-1}) which can be increased substantially (up to 2.1 S m^{-1}) using IL/molecular solvent mixtures. It is expected that these new thermally stable and low melting ionic liquids may have many new

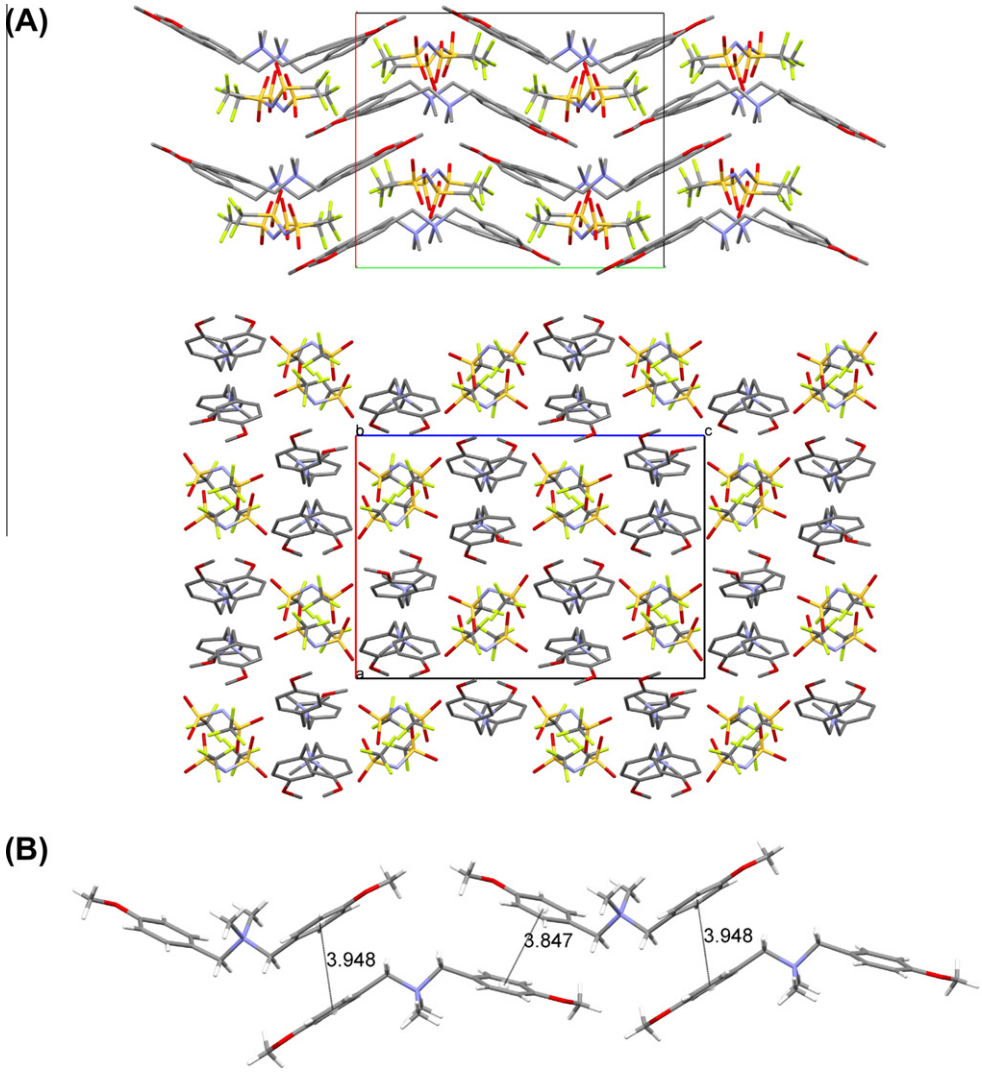

Fig. 9. (A) The packing of compound **4** up: viewed along the crystallographic *c*-axis. Down: along the *b*-axis. (B) Face to face π–π interactions forming the network of connections between cations. The anions have been removed for clarity.

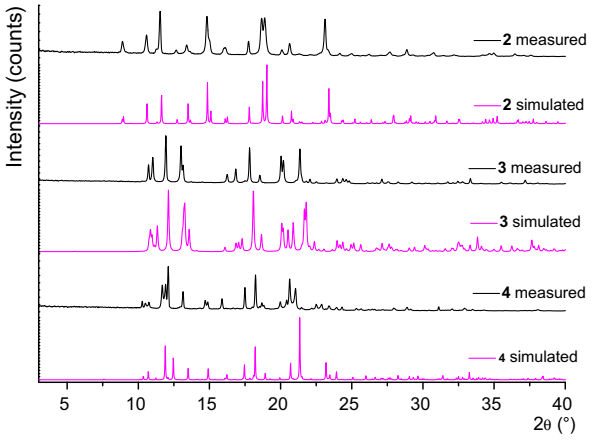

Fig. 10. Experimental PXDR patterns of **2** and **3** and **4** compared with simulated data, which are from the single crystal structure parameters.

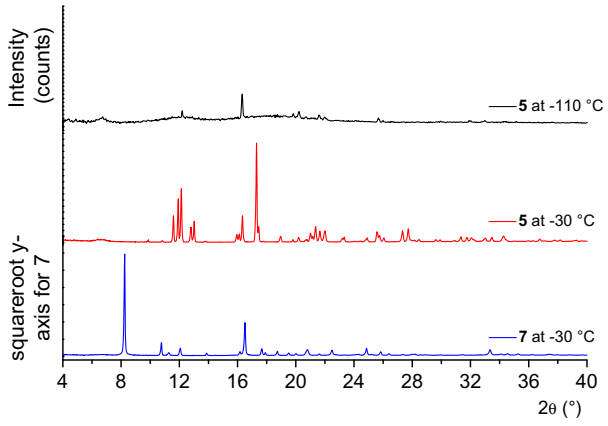

Fig. 11. The powder diffraction patterns of compound **5** (−110 and −30 °C) and **7** (at −30 °C) measured by *in situ* low-temperature X-ray diffraction.

perspectives in various fields of applications such as, heat transfer fluids, electrolytes (for instance dye-sensitized solar cells on which they will be tested in near future), high temperature synthesis solvents and lubricants.

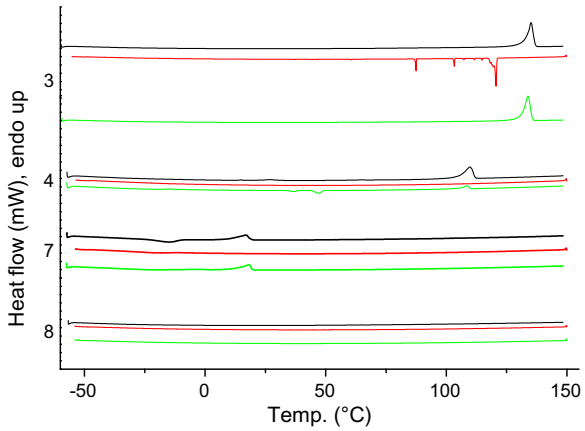

Fig. 12. DSC-curves for salts **3**, **4**, **7** and **8**.

Table 3
Thermal properties of compounds **1**–**8**.

Comp	M.W.	1st Heating scan	2nd Heating scan		Decomp.
		T_m and ΔH	T_g and ΔC_p	T_m and ΔH	T_d
1	506.48	101.71 (23.7)	–	101.42 (24.3)	306
2	534.54	78.66 (33.2)	–	77.60 (25.7)	295
3	534.54	132.99 (31.5)	–	131.05 (30.0)	277
4	566.54	105.31 (23.1)	−18.51 (0.2)	105.59 (4.2)	244
5	454.45	−1.65 (21.4)	−84.10 (0.1)	−1.65 (20.9)[a]	320
		14.98 (21.7)[b]	−84.2 (0.1)[b]	15.11(21.5)[b]	
6	496.53	62.08 (30.4)	–	58.72 (31.8)	294
7	538.61	9.76 (9.0)	–	10.29 (00.8)	282
8	580.69	–	−68.66 (0.2)	–	279

T_m = melting temperature, T_g = glass transitions temperature, ΔH = enthalpy of a transition (kJ mol^{-1}), ΔC_p = heat capacity change [kJ mol^{-1} °C^{-1}], T_d = decomposition onset by TG/DTA.

[a] Exhibits cold crystallization (crystallization on heating) between glass transition and melting.

[b] Show also two polymorphs depending on the cooling rate.

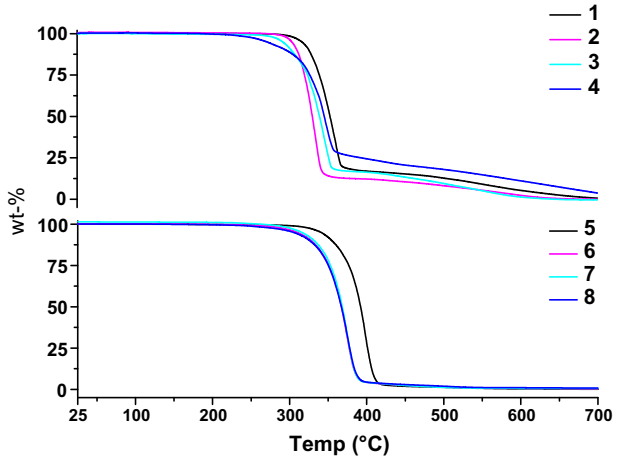

Fig. 13. TG curves of compounds **1–8** measured under air with heating rate of 5 °C/min.

Acknowledgements

We thank Ms. Elina Hautakangas for the elemental analyses, Mr. Reijo Kauppinen for the NMR-measurements and Ms. Mirja Lahtiperä for the ESI TOF MS-measurements. M.K. gratefully acknowledges the financial support of the Inorganic Materials Chemistry Graduate Program.

Appendix A. Supplementary material

Supporting information includes details of capillary electrophoresis measurements, additional PXRD patterns and DSC-scans. CCDC 775,442, 775,443 and 780,593 contains the supplementary crystallographic data for this paper. These data can be obtained free of charge from The Cambridge Crystallographic Data Centre via www.ccdc.cam.ac.uk/data_request/cif. Supplementary data associated with this article can be found, in the online version, at doi:10.1016/j.molstruc.2010.08.036.

References

[1] K.R. Seddon, J. Chem. Technol. Biotechnol. 68 (1997) 351–356.
[2] T. Welton, Chem. Rev. 99 (1999) 2071–2083.
[3] J.D. Holbrey, K.R. Seddon, Clean Prod. Proc. 1 (1999) 223–236.
[4] M.J. Earle, K.R. Seddon, Pure Appl. Chem. 72 (2000) 1391–1398.
[5] R. Sheldon, Chem. Commun. (2001) 2399–2407.
[6] P. Wasserscheid, T. Welton (Eds.), Ionic Liquids in Synthesis, second ed., Wiley-VCH, Germany, 2008.
[7] S.T. Handy, Chem. Eur. J. 9 (2003) 2938–2944.
[8] L. Ferguson, P. Scovazzo, Ind. Eng. Chem. Res. 46 (2007) 1369–1374.
[9] A. Grosse Boewing, A. Jess, Chem. Eng. Sci. 62 (2007) 1760–1769.
[10] G.J. Kemperman, T.A. Roeters, P.W. Hilberink, Eur. J. Org. Chem. (2003) 1681–1686.
[11] A. Marra, A. Vecchi, C. Chiappe, B. Melai, A. Dondoni, J. Org. Chem. 73 (2008) 2458–2461.
[12] A. Vecchi, B. Melai, A. Marra, C. Chiappe, A. Dondoni, J. Org. Chem. 73 (2008) 6437–6440.
[13] V. Kumar, S.V. Malhotra, Bioorg. Med. Chem. Lett. 19 (2009) 4643–4646.
[14] T. Sato, G. Masuda, K. Takagi, Electrochim. Acta. 49 (2004) 3603–3611.
[15] K. Yuyama, G. Masuda, H. Yoshida, T. Sato, J. Power Sources 162 (2006) 1401–1408.
[16] H. Zheng, G. Liu, V. Battaglia, J. Phys. Chem. C. 114 (2010) 6182–6189.
[17] T. Sato, T. Maruo, S. Marukane, K. Takagi, J. Power Sources 138 (2004) 253–261.
[18] C. Samori, A. Pasteris, P. Galletti, E. Tagliavini, Environ. Toxicol. Chem. 26 (2007) 2379–2382.
[19] S. Stolte, J. Arning, U. Bottin-Weber, A. Mueller, W. Pitner, U. Welz-Biermann, B. Jastorff, J. Ranke, Green Chem. 9 (2007) 760–767.
[20] L.C. Branco, J.N. Rosa, J.J.M. Ramos, C.A.M. Afonso, Chem. Eur. J. 8 (2002) 3671–3677.
[21] Q. Liu, M.H.A. Janssen, F. van Rantwijk, R.A. Sheldon, Green Chem. 7 (2005) 39–42.
[22] Z. Zhou, H. Matsumoto, K. Tatsumi, Chem. Eur. J. 11 (2005) 752–766.
[23] W.A. Henderson, V.G. Young Jr., D.M. Fox, H.C. De Long, P.C. Trulove, Chem. Commun. (2006) 3708–3710.
[24] H.S. Schrekker, M.P. Stracke, C.M.L. Schrekker, J. Dupont, Ind. Eng. Chem. Res. 46 (2007) 7389–7392.
[25] H.S. Schrekker, D.O. Silva, M.A. Gelesky, M.P. Stracke, C.M.L. Schrekker, R.S. Goncalves, J. Dupont, J. Braz. Chem. Soc. 19 (2008) 426–433.
[26] L.J.A. Siqueira, M.C.C. Ribeiro, J. Phys. Chem. B. 113 (2009) 1074–1079.
[27] X. Yang, Z. Fei, T.J. Geldbach, A.D. Phillips, C.G. Hartinger, Y. Li, P.J. Dyson, Organometallics 27 (2008) 3971–3977.
[28] M. Kärnä, M. Lahtinen, P. Hakkarainen, J. Valkonen, Aust. J. Chem. 63 (2010) 1122–1137.
[29] M. Kärnä, M. Lahtinen, J. Valkonen, J. Mol. Struct. 922 (2009) 64–76.
[30] S. Busi, M. Lahtinen, H. Mansikkamäki, J. Valkonen, K. Rissanen, J. Solid State Chem. 178 (2005) 1722–1737.
[31] S. Busi, M. Lahtinen, J. Ropponen, J. Valkonen, K. Rissanen, J. Solid State Chem. 177 (2004) 3757–3767.
[32] J. Ropponen, M. Lahtinen, S. Busi, M. Nissinen, E. Kolehmainen, K. Rissanen, New J. Chem. 28 (2004) 1426–1430.
[33] S. Busi, M. Lahtinen, M. Kärnä, J. Valkonen, E. Kolehmainen, K. Rissanen, J. Mol. Struct. 787 (2006) 18–30.
[34] Z. Otwinowski, W. Minor, Methods Enzymol. 276 (1997) 307–326.
[35] Z. Otwinowski, D. Borek, W. Majewski, W. Minor, Acta Crystallogr. Sect. A: Found. Crystallogr. A59 (2003) 228–234.
[36] G.M. Sheldrick, SADABS, Multi-Scan Absorption Correction Program, Version 2, 2001.
[37] G.M. Sheldrick, Acta Crystallogr. Sect. A: Found. Crystallogr. A46 (1990) 467–473.
[38] M.C. Burla, R. Caliandro, M. Camalli, B. Carrozzini, G.L. Cascarano, L. De Caro, C. Giacovazzo, G. Polidori, R. Spagna, J. Appl. Crystallogr. 38 (2005) 381–388.
[39] G.M. Sheldrick, Acta Crystallogr. Sect. A: Found. Crystallogr. A64 (2008) 112–122.
[40] K. Brandenburg, Crystal Impact GbR, Bonn, Germany, 2005.

[41] C.F. Macrae, P.R. Edgington, P. McCabe, E. Pidcock, G.P. Shields, R. Taylor, M. Towler, J. van de Streek, J. Appl. Crystallogr. 39 (2006) 453–457.
[42] C.A. Angell, J. Phys. Chem. Solids 49 (1988) 863–871.
[43] W. Xu, E.I. Cooper, C.A. Angell, J. Phys. Chem. B 107 (2003) 6170–6178.
[44] J. Belieres, C.A. Angell, J. Phys. Chem. B 111 (2007) 4926–4937.
[45] M. Anouti, M. Caillon-Caravanier, Y. Dridi, H. Galiano, D. Lemordant, J. Phys. Chem. B 112 (2008) 13335–13343.
[46] M. Anouti, M. Caillon-Caravanier, C. Le Floch, D. Lemordant, J. Phys. Chem. B 112 (2008) 9412–9416.
[47] I. Bandres, B. Giner, I. Gascon, M. Castro, C. Lafuente, J. Phys. Chem. B 112 (2008) 12461–12467.
[48] C. Brigouleix, M. Anouti, J. Jacquemin, M. Caillon-Caravanier, H. Galiano, D. Lemordant, J. Phys. Chem. B 114 (2010) 1757,1758–1766.
[49] C.T. Moynihan, P.B. Macedo, C.J. Montrose, P.K. Gupta, M.A. DeBolt, J.F. Dill, B.E. Dom, P.W. Drake, A.J. Easteal, et al., Ann. N. Y. Acad. Sci. 279 (1976) 15–35.
[50] A. Boultif, D. Louer, J. Appl. Crystallogr. 37 (2004) 724–731.
[51] P.M. de Wolff, J. Appl. Crystallogr. 1 (1968) 108–113.
[52] W.I.F. David, K. Shankland, J. van de Streek, E. Pidcock, W.D.S. Motherwell, J.C. Cole, J. Appl. Crystallogr. 39 (2006) 910–915.
[53] P.S. Kulkarni, L.C. Branco, J.G. Crespo, M.C. Nunes, A. Raymundo, C.A.M. Afonso, Chem. Eur. J. 13 (2007) 8478–8488.